Carcinogenesis Advance Access published July 19, 2010

microRNAome changes in bystander three-dimensional human tissue models suggest priming of apoptotic pathways

Olga Kovalchuk[#], Franz J. Zemp[#], Jody Filkowski[#], Alvin Altamirano[#], Jennifer S. Dickey*, Gloria Jenkins-Baker[†], Stephen A. Marino[†], David J. Brenner[†], William M. Bonner*, Olga A. Sedelnikova*

[#]Department of Biological Sciences, University of Lethbridge, 4401 University Drive, Lethbridge, AB, T1K 3M4 Canada

[†] Radiation Accelerator Research Facility, Center for Radiological Research, Columbia University, 630 West 168th St., New York, NY, 10032

* Laboratory of Molecular Pharmacology, Center for Cancer Research, NCI, NIH, 9000 Rockville Pike, Bethesda, MD, 20892

Running Title: *microRNAome in bystander 3-D tissue models*

Key Words: bystander effect, α-particle microbeam irradiation, microRNA analysis, 3-D tissue models

Financial support: [#] National Science and Engineering Research Council of Canada; [†]The National Institute of Biomedical Imaging and Bioengineering under grant: NIBIB 5 P41 EB002033-12; *Intramural Research Program of the National Cancer Institute, Center for Cancer Research, NIH, and the NIAID Radiation/Nuclear Countermeasures Program and the Intramural Research Program of the National Cancer Institute, Center for Cancer Research, NIH.

Reprint requests should be sent to: Olga Kovalchuk, University of Lethbridge, Lethbridge, AB, Canada. Phone: 403 394 3916; Fax: 403 329 2242; E-mail: olga.kovalchuk@uleth.ca

Abstract

The radiation-induced bystander effect (RIBE) is a phenomenon whereby unexposed cells exhibit molecular symptoms of stress exposure when adjacent or nearby cells are traversed by ionizing radiation (IR). Recent data suggest that RIBE may be epigenetically mediated by microRNAs (miRNAs), which are small regulatory molecules that target mRNA transcripts for translational inhibition. Here we analyzed microRNAome changes in bystander tissues after α-particle microbeam irradiation of three-dimensional artificial human tissues using microRNA microarrays. Our results indicate that IR leads to a deregulation of miRNA expression in bystander tissues. We report that major bystander endpoints, including apoptosis, cell cycle deregulation, and DNA hypomethylation, may be mediated by altered expression of miRNAs. Specifically, c-MYC-mediated upregulation of the miR-17 family was associated with decreased levels of E2F1 and RB1, suggesting a switch to a proliferative state in bystander tissues, while priming these cells for impending death signals. Upregulation of the miR-29 family resulted in decreased levels of its targets DNMT3a and MCL1, consequently affecting DNA methylation and apoptosis. Altered expression of miR-16 led to changes in expression of BCL2, suggesting modulation of apoptosis. Thus, our data clearly show that miRNAs play a profound role in the manifestation of late RIBE endpoints. In summary, this study creates a roadmap for understanding the role of microRNAome in RIBE and for developing of novel RIBE biomarkers.

Introduction

Bystander effects are non-targeted effects of radiation whereby unexposed cells exhibit the molecular symptoms of stress exposure when adjacent or nearby cells are traversed by ionizing radiation (IR). To date, a variety of radiation-induced bystander effect (RIBE) studies have been performed using cell culture models [1-4]. However, these experiments utilized cell cultures in a single monolayer, making extrapolation to human exposure somewhat difficult. Recent work in tissue explants [5,6], spheroids [7], three-dimensional (3-D) cell cultures [8], and 3-D artificially reconstructed human tissues [9,10] have suggested that the cell-cell bystander effect operates in human 3-D systems. Thus, the RIBE remains an important and relevant consideration in the study of radiobiology.

RIBE encompass a wide range of genetic alterations, including gross genome rearrangements, chromosome aberrations, sister chromatid exchanges, deletions, duplications, mutations, and amplifications (reviewed in [11-15]). These effects also influence gene expression, cellular proliferation, cell cycle regulation, senescence, and cell death [10,11], and are believed to be linked to IR-induced genome instability [13]. However, while a great deal of data confirms the existence and manifestation of RIBE in cultured cells and 3-D tissues, the mechanisms are yet to be discovered.

The high frequency of induction and occurrence, as well as persistence of RIBE has led some to suggest that epigenetic regulation may play an important role in bystander cells and tissues [10,16,17]. Epigenetic changes are alterations in gene expression induced by DNA methylation, histone modifications, and RNA-associated silencing [18]. MicroRNAs (miRNAs) are important components of the RNA-associated silencing machinery. MiRNAs are small regulatory molecules known to target mRNA transcripts for translational inhibition or, rarely, degradation in humans [19]. Since their discovery, miRNAs have been found to play essential roles in regulating processes such as terminal differentiation [20], cell cycle [21], apoptosis [22], and DNA methylation [23]. Further, genotoxic

stress exposure deregulates cellular miRNA expression [24-26]. Logically, deregulation of these miRNAs has been associated with a number of diseases, including cancer.

Based on the importance of miRNAs in the modulation of various cellular processes and the fact they have been shown to be regulated in *in vivo* RIBE [24,27], we decided to analyze microRNAome changes in bystander tissues after α-particle microbeam irradiation of three-dimensional artificial human tissues using microRNA microarrays. Microarray data analysis has indicated that some of the molecular endpoints previously found in this bystander model may be the result of changes in miRNA expression. Our data suggest that miRNA regulation acting in concert with c-Myc activation in bystander tissues may sensitize bystander cells to apoptosis.

Materials and Methods

Tissue systems and culture

These experiments utilized a human 3-D tissue culture system (MatTek Corp, Ashland, MA). These artificial tissues reconstruct the normal tissue microarchitecture and preserve the *in vivo* differentiation patterns. They are mitotically and metabolically active, capable of releasing relevant cytokines, and contain gap junctions [28]. They are stable and allow a high degree of experimental reproducibility [9,10]. Specifically, we employed the EpiAirway™ (Air-112) tissue model (Fig. 1). The tissues were cultured according to the manufacturer's protocol, using an air-liquid interface tissue culture technique.

Microbeam irradiation and delivered dose calculations

The Columbia University RARAF Singletron accelerator was used to produce a broad beam of ^{4}He ions with an initial energy of 8.6 MeV. The ions passed through a Mylar scattering foil and a Havar metal vacuum window (together ~20 μm-thick), and 8 μm of air before entering the membranes on which tissue samples were grown.

Each tissue culture insert was placed on a plastic disc that had a hole in the center. Two 50 μm stainless steel half-discs (sufficient to stop ^{4}He ions) were glued over each hole with a 25 μm gap between them. This allowed a single plane of tissue to be irradiated from below through the membrane that forms the base of the culture insert. The discs were placed on an irradiation wheel and rotated across the beam. The slits through which the tissue samples were irradiated were aligned with the direction of rotation so that there was almost no variation in the dose across the sample.

Assuming the pores of the Teflon sponge membrane were filled with tissue medium, ^{4}He ions had the energy of ~4.5 MeV, LET values of ~110 keV/μm and the range of ~30 μm at the membrane-tissue interface. The tissue is thicker than the range of ^{4}He ions. As the ions penetrate the tissue, their LET increases to approximately 230 keV/μm just before they stop. Doses were measured using an ionization chamber with a Mylar window filled with methane-based tissue equivalent gas. Based on a nuclear diameter of 5 μm, cell nuclei were irradiated with approximately 5 ^{4}He ions per nucleus. Calculations of ^{4}He ion energy, LET and range were made for the irradiation conditions using tables of ranges and stopping powers for ^{4}He ions generated by the computer program SRIM-2008 [29] . The estimated dose for the first layer of cells is 5.4 Gy.

After irradiation, each tissue sample was returned to a multi-well dish filled with fresh medium and incubated at 37°C in a humidified atmosphere of 5% CO_2. Tissues were removed and frozen on dry ice at 8 hrs and 1, 2, 3, 4, 5, and 7 days post-IR. Time-matched, mock-treated controls were available 8 hrs, 3 days, and 7 days post-mock IR. Mock-treated tissue frozen at the time of IR established the base-line expression level. The tissues were stored at -80°C before microdissection and RNA and protein extraction.

Tissue microdissection and RNA extraction

The line of irradiation was marked on the insert. Frozen tissues were placed on a liquid N_2-chilled glass plates. Scalpels were used to cut ~1-1.5 mm slabs from the center of the tissues along the

irradiated plane to secure the bystander remaining tissues (~ 2 mm-thick on either side of the slabs) (Fig. 1). The center slabs of the tissues represented mixed irradiated and bystander cell layers. The soley bystander tissues from either side of the slabs were pooled to a single microfuge tube.

Targeted and bystander tissues can be distinguished based on differences in kinetics of IR-induced and bystander DSB formation and repair marked by the γ-H2AX antibody[30] . Earlier we reported that in marked contrast to DNA DSB dynamics in directly irradiated cells, in which maximal DSB formation was seen 30 min post-IR, the incidence of DSBs in bystander tissues reached a maximum much later, by 12 to 48 hrs post-IR [10]. Thus the central regions of the tissues (the 1.5 mm slabs containing irradiated planes of the tissues as well as un-irradiated cells) show biphasic γ-H2AX focal kinetics, while bystander tissues exhibit the bystander-like delayed γ-H2AX focal kinetics providing additional verification of bystander tissue identity (Suppl. Fig. 1).

miRNA expression profiling

Three biological replicates were used for each of the experimental time points and treatment conditions. The bystander and mock-treated tissues were immersed in TRIzol (500 μL), and the samples were vortexed for 5-10 seconds to remove the tissues from the membrane. RNA extraction was carried out as per the manufacturer's protocol (TRIzol, Invitrogen, Carlsbad, CA). The miRNA microarray analysis was performed by LC Sciences (Houston, TX) as a paid service as previously described [24,26].

In brief, total RNA (10 μg) was size-fractionated (<200 nucleotides) using a mirVana kit (Ambion) and labeled with Cy3 and Cy5 fluorescent dyes. Dye switching was performed to eliminate any dye bias. Pairs of labeled samples were hybridized to dual-channel microarrays. Microarray assays were carried out on a ParaFlo microfluidics chip. Each of the detection probes on the chip contained a nucleotide sequence of coding segment complementary to a specific miRNA sequence and a long nonnucleotide molecule spacer that extended the detection probe away from the substrate [31]. The miRNA detection signal threshold was defined as twice the maximum background signal. The

maximum signal level of background probes was 180. To remove any system-related variations normalization was performed using a cyclic LOWESS (locally weighted regression) method [32]. Data adjustments included data filtering, log2 transformation, and gene centering and normalization. The t-test and ANOVA analyses were conducted between the sample groups, samples, and miRNA with P values < 0.05 were selected for cluster analysis. The clustering analysis was done using a hierarchical method, average linkage, and Euclidean distance metrics [31,33].

Western blotting

Protein extraction and western blotting was conducted as described [26,27]. Membranes were incubated with antibodies against MYC, E2F1, RB1, DNMT3a, BCL2 (1:500; Santa Cruz Biotechnology, Santa Cruz, CA), MCL1 (1:1000; Cell Signalling, Bedford, MA) and actin (1:2000; Santa Cruz Biotechnology). Antibody binding was revealed by incubation with horseradish peroxidase-conjugated secondary antibodies and the ECL Plus immunoblotting detection system (GE Healthcare, Piscataway, NJ). Chemiluminescence was detected by Biomax MR film (Eastman Kodak, New Haven, CT) and scanned. Samples were loaded in a random manner to insure lack of bias. For presentation purposes, after scanning pictures were arranged in the following order: mock 8 hours; bystander 8 hours; mock 3 days; bystander 3 days; bystander 5 days.

Immunohistochemistry

Frozen tissues were sectioned into 5-10 μm-thick slices, which were perpendicular to the plane of the irradiated cells. Frozen sections were dried, fixed in 2% paraformaldehyde, permeabilized with 1% Triton X-100 and processed for immunostaining with a rabbit polyclonal ant-cleaved caspase-3 antibody (Trevigen, Gaithersburg, MD) and mouse monoclonal anti-γ-H2AX antibody (Abcam, Cambridge, MA) as previously described[34] . Frequencies of cleaved caspase-3–positive cells were recorded for at least 1,000 cells of side section areas. γ-H2AX foci were recorded by collapsing 0.5 μm

optical Z-sections through the nuclei in a single plane and counting by eye in a blinded fashion in 100-200 randomly chosen cells of central and side areas of sections.

Statistical analysis

Statistical analysis was conducted using Student's *t*-test. P-values <0.05 were considered significant.

Results

miRNAome deregulation in bystander tissues

We employed the EpiAirway™ (Air-112) tissue model, which consists of normal, human-derived tracheal/bronchial epithelial cells that have been cultured to form a highly differentiated model that closely resembles the epithelial tissue of the respiratory tract. Fig. 1 displays tissue dimensions and the location of irradiated and bystander tissues. In this model, the targeted and bystander tissues can be distinguished based on the different kinetics of IR-induced and bystander DSB formation and repair marked by the γ-H2AX antibody [10].

To analyze the role of the microRNAome in RIBE, miRNA expression profiles of bystander tissues were compared to time-matched mock controls at 8 hrs, 3 days and 7 days post-IR (dpi). MiRNAs were considered for comparison only if their average expression levels were over 1000 arbitrary units of fluorescence (AUF). The reason for this was three-fold. Firstly, miRNAs with very low expression levels, <1000 AUF, are analyzed with less sensitivity by conventional microarray methods. Secondly, downstream studies involving qRT-PCR methods are limited to miRNAs with expression levels of >1000 AUF. Finally, fold induction of miRNAs with low expression levels is less biologically significant than of those with higher expression levels.

At 8 hrs post-IR (8 hpi), four miRNAs (Student's *t*-test, $p<0.05$) changed significantly in bystander tissue over the time-matched controls. These were miR-22, -141, and -16 which were 2.0-, 1.8-, and 1.2-fold up-regulated, and miR-183 which was 1.3-fold down-regulated (Table 1). At 3 dpi,

six miRNAs were found to be significantly different from the mock control; miR-29a, -29c, -30a-5p, and -20a were 2.45-, 1.62-, 1.47-, and 1.25-fold up-regulated, respectively, while miR-146a and -125b appeared to be 1.26-, and 1.18-fold down-regulated, respectively. The final time point, 7 dpi, yielded only two significantly regulated miRNAs, miR-181a and -181b, which were 1.5- and 1.2-fold down-regulated (Table 1). These fold changes in miRNA expression over the time-course may initially seem small, but it is important to keep in mind that only a very small area of the tissue was actually irradiated. The signalling capacity of RIBE in terms of distance has not been precisely defined in this model. Thus, as all non-irradiated tissue used in this study was harvested as bystander tissue, some of the fold-inductions may be diluted. Unfortunately, these tissue models are too scarce to be used in *in situ* miRNA analysis of selected miRNAs.

We examined expression levels of selected miRNAs at all time-points after exposure and at available time-matched controls. This allowed us to establish an expression trend over the experimental period. Next, we analyzed patterns of microRNA expression at all time-points based on ANOVA analysis. The ANOVA-based expression patterns from all treatment groups can be seen in the heat map ($p<0.05$; Fig. 2). These miRNAs were clustered according to expression patterns. Viewing the array in this manner has revealed very intriguing groups of inter-related miRNAs. Amongst those, the miR-17-92 and mir-29 families exhibited the most interesting expression patterns.

Altered expression of the miR-17-92 family and deregulation of RB1 and E2F levels in bystander tissues

We identified a group of significantly changed miRNAs, including miR-106a, -106b, -17-5p, -20a, and -19b that all belong to the same miR-17-92 family (Fig. 2). Interestingly, this family has members that reside in three separate polycistrons on different chromosomes. The miR-17 cluster is located on chromosome 13 [13: 90800860-90801646 (+)]and consists of miR-17, -18a, -19a, -20a, 19b-1, and 92-1. The 106a cluster on chromosme X [X:133131148-133131894 (-)] is composed of miR-106a, -20b, -19b-2, -92-2, and -363. Finally, the mir-106b cluster composed of 106b, 93,25 is located

on chromosome 7 [7:99529202-99528552 (-)] and contains miR-106b, 93, and 25. Both clusters 17 and 106a are intergenic, while the 106b cluster is located in intron 11 of the *MCM7* gene. The regulation of this miRNA group in bystander tissues consisted of an initial increase at 8 hpi that persisted before returning to control levels at 7 dpi (Fig. 2, Suppl. Fig. 2).

Due to the similar regulation of these miRNAs located on different chromosomes, it is possible that they have similar regulatory elements. Both the miR-17 and -106b promoters have been predicted to be regulated by the c-MYC transcription factor [35,36].

To see if c-MYC was deregulated in bystander tissues, we performed Western blot analysis to assess protein levels. We observed an increased level of c-MYC in bystander tissues, suggesting that c-MYC upregulation mediates upregulation of the miR-17-92 family in bystander tissues (Fig. 3). Further, the miR-17-92 family members are known to be oncogenic miRNAs, and they have found to be deregulated in a number of cancers [37]. The miR-17-92 family is also known to regulate E2F transcription factors via miR-20a and miR-17-5p and possibly other miRNAs in these clusters. Interestingly, the E2F transcription factors are also induced by c-MYC and, conversely, c-MYC is induced by E2Fs [38]. Importantly, in this study we observed a notable up-regulation of MYC and the miR-17-92 cluster, and down-regulation of E2F1 in bystander tissues (Fig. 3, Fig. 4 A).

Further, the miR-106 miRNAs have been shown to target retinoblastoma protein (RB1) [39], a well-known cell cycle regulator protein [40]. Interestingly, the up-regulation of miR-106 suggests a down-regulation of RB1. Analyzing the levels of RB1 in bystander tissue, we found that the upregulation of miR-106 was correlated with down-regulation of RB1 (Fig. 4A).

MiR-16-mediated regulation of BCL2 in bystander tissues

MiR-16 was up-regulated at 8 hpi in bystander tissues (Table 1), however, miR-16 expression showed a strong trend of upregulation for the duration of the experiment until day 7 where it returns to control levels (Fig. 2).

It has been shown that miR-16 targets BCL2, a well-known anti-apoptotic protein and it is the overexpression of BCL2 that largely contributes to the malignant phenotype in chronic lymphocytic leukemia [41]. Here we show that miR-16 is up-regulated, suggesting cellular BCL2 levels would be lower, which indeed is the case (Fig. 4B). Despite the absence of increased rates of apoptosis in the previous experiments at this time point, the elevated levels of BCL2 could induce a pro-apoptotic state in these cells, increasing their susceptibility to signalled cell death.

The miR-29 family affects MCL1 and DNMT3a and influences apoptosis and DNA hypomethylation in bystander tissues

The miR-29 family members are situated at two separate intergenic loci, miR-29a and -29b-1 on chromosome 7 [7:130212046-130212838 (-)] and miR-29c and -29b-2 on chromosome 1 [1:206041820-206042491 (-)]. MiR-29a and -29c are significantly upregulated in bystander tissues at 3 dpi. Mir-29b is also upregulated but with less confidence ($p<0.10$). Thus, the entire family follows the same overall expression trends in bystander tissues (Fig. 2).

MiR-29a was the most highly affected miRNA in the array. Though its fold induction was not the highest observed, it had the largest absolute change in expression, from ~12,000 AUF in control cells to ~20,000 AUF in bystander cells. Considering the competition for the miRNA machinery in the cell, it is likely that a change of this magnitude is more biologically significant than higher-fold induction in less-expressed miRNAs; for example, a 5-fold change of 50 AUF to 250 AUF.

The miR-29 family has been well characterized in humans and has some very interesting and relevant targets. The miR-29 family targets MCL1, a tightly controlled BCL2 family member which is important in regulating tumour necrosis factor (TNF)-related apoptosis-inducing ligand (TRAIL)-mediated apoptosis [42]. In this study, up-regulated levels of miR-29 members were paralleled by down-regulation of MCL1 in bystander tissues (Fig. 4B). Therefore, we suggest that significant up-regulation of the miR-29 family in bystander tissues may be sensitizing or priming them for apoptosis. In agreement with our previous data based on this bystander model [10], apoptotic levels reached a

maximum 3 and 4 dpi before returning to basal levels at 7 dpi. These increases in apoptosis over the experimental period closely mirror the expression level of the miR-29 family over the same experimental period, further suggesting an important role of miR-29s and MCL1 in the regulation of apoptotis. As the next step of our study we analyzed the levels of apoptosis by scoring the number of cells positive for cleaved caspase 3. Analysis revealed significantly ($P<0.05$) elevated levels of apoptosis in bystander cells 3 dpi (Fig. 5). The miR-29 family also influences *de novo* DNA methyltransferases DNMT3a and DNMT3b. Fabbri and colleagues have shown that the miR-29 family targets these methyltransferases and leads to aberrant methylation patterns [23]. These data suggest that miR-29 expression can directly affect methylation patterns, and the possibility of this regulation in bystander tissues is a truly novel finding. We have previously reported that IR leads to hypomethylation in 3-D tissue models of RIBE [10]. Here we show that this hypomethylation corresponds to decreased levels of DNMT3a and increased levels of the miR-29 family in bystander tissues (Fig. 4C).

Interestingly, in our previous experiments DNA hypomethylation levels in bystander tissues peaked at 3 dpi and declined at 7 dpi [10], a trend that is also mimicked by miR-29 expression observed in the current experiment. These data show that miR-29 family expression is very well correlated with DNMT3a protein levels. These factors may be responsible for hypomethylation previously seen in this bystander model.

Discussion

In this study, we analyzed microRNAome changes in bystander tissues in an '*in vivo*' EpiAirway human tissue model. Bystander tissues in this model display profound cellular and molecular changes [9,10]. Specifically, previous research showed an increase in apoptosis, DNA DSBs, micronucleus formation, and cellular senescence as well as a decrease in global genome methylation. Additionally, RIBE is associated with deregulation of cell cycle control. Given that miRNAs are known to regulate some of these processes, we investigated the roles that miRNAs may play in the bystander

response. Importantly, we found that major RIBE endpoints – apoptosis, cell cycle deregulation, and global genome hypomethylation may be mediated by altered expression of miRNAs (Fig. 6).

Furthermore, we also show that altered miRNA expression in bystander tissues may be due to the bystander-induced expression of c-MYC. c-*MYC* is a widely studied gene involved in the control of cell size, cell cycle, proliferation, and apoptosis [43]. It has been shown that the proto-oncogene c-MYC transcription factor binds the miR-17-92 cluster's promoter region, inducing these miRNAs to target E2F transcripts [35]. The current paradigm is that the miR-17-92 cluster works as a regulator of a positive feedback loop between c-MYC and E2F transcription factors, preventing a reciprocal positive feedback from 'runaway' regulation [44]. The up-regulation of the miR-17-92 cluster via c-MYC to cause elevated expression levels of miR-17 and -20a is thought to indicate environmental signals to switch the cell to a proliferative state [44]. Our study shows that up-regulation of MYC and the miR-17-92 cluster and down-regulation of E2F1 in bystander tissues, supportive of the current paradigm. Furthermore, we found that the upregulation of miR-106 was correlated with down-regulation of RB1.

It is interesting to speculate on the function of c-MYC activity in bystander tissues. Increased levels of c-MYC in the cell are most often associated with deregulated cell cycle and increased cellular proliferation, and the regulation of many miRNAs in the miR-17 family in bystander tissues suggests that this may be the case. Unfortunately, due to the scarcity of tissues, an increase in cellular proliferation in this bystander model has not been assayed, although it has been found in some bystander models [12-14]. Future experiments in this model should assay whether cell proliferation actually occurs in bystander cells, or whether the cell is just 'poised' to proliferate after further extracellular signals.

We can also look at these changes in cellular alignment governed by c-MYC and the miR-17 family in a different way that is more commonly associated with bystander effects. It is thought that c-MYC may prime the cell for apoptosis [45,46]. Taken in this context, upregulation of c-Myc in these

tissues may sensitize bystander cells for an impending death signal. Indeed, we have noted a significant increase in the level of apoptotic cells in bystander issues.

Further, c-MYC and BCL2 have long been shown to associate with cancer cells, whereby it is usually the overexpression of both that leads to the cancer phenotype. The result of this cooperation is that BCL2 suppresses c-MYC driven apoptosis [45-47]. However, our miRNA and protein expression patterns lead us to believe that BCL2 is down-regulated via the action of miR-16. MiR-16 is significantly up-regulated at 8 hpi, with a strong trend towards up-regulation at 3 dpi (Fig. 2). It is possible that this decrease in cellular BCL2 is functioning to accent c-MYC directed priming of apoptosis.

Moreover, apoptosis in bystander cells is also regulated via the miR-29 family, which mediates apoptosis through the regulation of MCL1. MCL1 is a tightly controlled BCL2 family member which is important in regulating TRAIL-mediated apoptosis [42]. MCL1 functions as a pro-survival protein by binding pro-apoptotic BH3-only BCL2 family members, such as BIM, BID, BIK, NOXA, and PUMA [48]. Although the exact mechanisms by which the BCL2 family members mediate apoptosis is unknown, it has been shown that MCL1 binding of BID and BIM proteins protects against TRAIL-induced cell death [42]. Interestingly, it has been shown that TRAIL mediates cell-cell apoptotic RIBE [49,50]. This study and our previous analysis show that bystander cells exhibit increased levels of apoptosis. Furthermore, the data of this study may suggest that TNF-mediated cytokine signalling in RIBE may be associated with miR-29 family.

Overall, the miR-29 family plays a dual role in bystander tissues promoting both global hypomethylation through the regulation of *de novo* methyltransferases DNMT3A and preparing the cell for TRAIL-mediated apoptosis through repression of anti-apoptotic MCL1. We also show that miRNA regulation in bystander tissues has been dramatically changed at 3 dpi. Interestingly, this corresponds to the apoptotic levels observed in this study, and with the maximum apoptotic and hypomethylation levels previously seen in EpiAirway tissues under similar conditions [10]. Given that there are

significant changes in miRNA expression in bystander tissues, further investigation into the role of the miR-29 family in RIBE may come to discover that this family can acts as a good biomarker for two commonly observed bystander responses.

In previous experiments [10], there were no large-scale changes in molecular events at the 8 hpi time point. This is logical, as it takes time for the bystander signal to propagate through cells and for global cellular changes to manifest. However, finding changes in miRNA expression at early time points, before the manifestation of bystander symptoms, could suggest that miRNA regulation is an upstream event of some bystander responses. Given that miRNAs may travel through gap-junctions and gap-junctions are necessary for bystander effects in some models [51], one can easily envisage a future model where miRNAs from irradiated cells are quickly transported through gap-junctions to prepare bystander cells for future secreted signals.

Though miRNAs mediate crucial bystander effect endpoints and exhibit their effects as early as 8 hpi, they may not necessarily be primary bystander signals. Further studies are needed to dissect the potential role of miRNAs as bystander signals and to gain further mechanistic insight into the roles of miRNAs in irradiated and bystander tissues and the potential of miRNAs to enhance or suppress the RIBE *in vivo*. This challenging task can be achieved through transient transformation of irradiated and bystander cells and tissues using miRNAs or their inhibitors (antago-miRs or antimiRs) [52,53]. Following the transient transformation, the impact of miRNAs or anti-miRNAs on preventing or enhancing changes in the functional RIBE readouts can be established.

Interestingly, RIBE may be mediated by reactive oxygen species (ROS)[54]. A recent study has confirmed that IR-induced oxidative stress significantly alters microRNAome of the exposed cells [55]. Furthermore, the results clearly demonstrated that a common miRNA expression signature in response to radiation, hydrogen peroxide and etoposide exposure [55]. Though we have not seen a major overlap between our dataset and the reported IR- and ROS-induced miRNAs changes, some interesting parallels can be drawn. Specifically, miR-15b was up-regulated by IR and ROS, while in our study

miR-16 was significantly upregulated in bystander tissues. These miRNAs belong to the same miRNA family and play roles in regulation of cell cycle and apoptosis [56-58]. Their roles in ROS-induced bystander effects and their differential regulation in responses to direct IR and RIBE need to be further analyzed.

Overall, in the future, the current study may serve as a roadmap for further understanding the mechanistic roles of miRNAs in bystander effects, and for dissecting a hierarchy and crosstalk between epigenetic parameters (microRNAome and DNA methylation) and well-known RIBE manifestations.

ACKNOWLEDGEMENTS:

We appreciate the help of Dr. Valentina Titova in proofreading this manuscript.

Literature

1. Maguire, P., Mothersill, C., McClean, B., Seymour, C. and Lyng, F.M. (2007) Modulation of radiation responses by pre-exposure to irradiated cell conditioned medium. *Radiat Res*, **167**, 485-92.
2. Sokolov, M.V., Smilenov, L.B., Hall, E.J., Panyutin, I.G., Bonner, W.M. and Sedelnikova, O.A. (2005) Ionizing radiation induces DNA double-strand breaks in bystander primary human fibroblasts. *Oncogene*, **24**, 7257-65.
3. Lyng, F.M., Maguire, P., McClean, B., Seymour, C. and Mothersill, C. (2006) The involvement of calcium and MAP kinase signaling pathways in the production of radiation-induced bystander effects. *Radiat Res*, **165**, 400-9.
4. Gaugler, M.H., Neunlist, M., Bonnaud, S., Aubert, P., Benderitter, M. and Paris, F. (2007) Intestinal epithelial cell dysfunction is mediated by an endothelial-specific radiation-induced bystander effect. *Radiat Res*, **167**, 185-93.
5. Vines, A.M., Lyng, F.M., McClean, B., Seymour, C. and Mothersill, C.E. (2009) Bystander effect induced changes in apoptosis related proteins and terminal differentiation in in vitro murine bladder cultures. *Int J Radiat Biol*, **85**, 48-56.
6. Belyakov, O.V., Folkard, M., Mothersill, C., Prise, K.M. and Michael, B.D. (2006) Bystander-induced differentiation: a major response to targeted irradiation of a urothelial explant model. *Mutat Res*, **597**, 43-9.
7. Persaud, R., Zhou, H., Baker, S.E., Hei, T.K. and Hall, E.J. (2005) Assessment of low linear energy transfer radiation-induced bystander mutagenesis in a three-dimensional culture model. *Cancer Res*, **65**, 9876-82.
8. Pinto, M., Azzam, E.I. and Howell, R.W. (2006) Bystander responses in three-dimensional cultures containing radiolabelled and unlabelled human cells. *Radiat Prot Dosimetry*, **122**, 252-5.
9. Belyakov, O.V., Mitchell, S.A., Parikh, D., Randers-Pehrson, G., Marino, S.A., Amundson, S.A., Geard, C.R. and Brenner, D.J. (2005) Biological effects in unirradiated human tissue induced by radiation damage up to 1 mm away. *Proc Natl Acad Sci U S A*, **102**, 14203-8.
10. Sedelnikova, O.A., Nakamura, A., Kovalchuk, O., Koturbash, I., Mitchell, S.A., Marino, S.A., Brenner, D.J. and Bonner, W.M. (2007) DNA double-strand breaks form in bystander cells after microbeam irradiation of three-dimensional human tissue models. *Cancer Res*, **67**, 4295-302.
11. Morgan, W.F. and Sowa, M.B. (2007) Non-targeted bystander effects induced by ionizing radiation. *Mutat Res*, **616**, 159-64.
12. Morgan, W.F. (2003) Non-targeted and delayed effects of exposure to ionizing radiation: I. Radiation-induced genomic instability and bystander effects in vitro. *Radiat Res*, **159**, 567-80.
13. Morgan, W.F. (2003) Is there a common mechanism underlying genomic instability, bystander effects and other nontargeted effects of exposure to ionizing radiation? *Oncogene*, **22**, 7094-9.
14. Morgan, W.F. (2003) Non-targeted and delayed effects of exposure to ionizing radiation: II. Radiation-induced genomic instability and bystander effects in vivo, clastogenic factors and transgenerational effects. *Radiat Res*, **159**, 581-96.
15. Mothersill, C. and Seymour, C.B. (2004) Radiation-induced bystander effects--implications for cancer. *Nat Rev Cancer*, **4**, 158-64.
16. Kaup, S., Grandjean, V., Mukherjee, R., Kapoor, A., Keyes, E., Seymour, C.B., Mothersill, C.E. and Schofield, P.N. (2006) Radiation-induced genomic instability is associated with DNA methylation changes in cultured human keratinocytes. *Mutat Res*, **597**, 87-97.
17. Wright, E.G. and Coates, P.J. (2006) Untargeted effects of ionizing radiation: implications for radiation pathology. *Mutat Res*, **597**, 119-32.

18. Jaenisch, R. and Bird, A. (2003) Epigenetic regulation of gene expression: how the genome integrates intrinsic and environmental signals. *Nat Genet*, **33 Suppl**, 245-54.
19. Eulalio, A., Huntzinger, E. and Izaurralde, E. (2008) Getting to the root of miRNA-mediated gene silencing. *Cell*, **132**, 9-14.
20. Foshay, K.M. and Gallicano, G.I. (2007) Small RNAs, big potential: the role of MicroRNAs in stem cell function. *Curr Stem Cell Res Ther*, **2**, 264-71.
21. Carleton, M., Cleary, M.A. and Linsley, P.S. (2007) MicroRNAs and cell cycle regulation. *Cell Cycle*, **6**, 2127-32.
22. Jovanovic, M. and Hengartner, M.O. (2006) miRNAs and apoptosis: RNAs to die for. *Oncogene*, **25**, 6176-87.
23. Fabbri, M., Garzon, R., Cimmino, A., Liu, Z., Zanesi, N., Callegari, E., Liu, S., Alder, H., Costinean, S., Fernandez-Cymering, C., Volinia, S., Guler, G., Morrison, C.D., Chan, K.K., Marcucci, G., Calin, G.A., Huebner, K. and Croce, C.M. (2007) MicroRNA-29 family reverts aberrant methylation in lung cancer by targeting DNA methyltransferases 3A and 3B. *Proc Natl Acad Sci U S A*, **104**, 15805-10.
24. Koturbash, I., Zemp, F.J., Kutanzi, K., Luzhna, L., Loree, J., Kolb, B. and Kovalchuk, O. (2008) Sex-specific microRNAome deregulation in the shielded bystander spleen of cranially exposed mice. *Cell Cycle*, **7**, 1658-67.
25. Tamminga, J., Kathiria, P., Koturbash, I. and Kovalchuk, O. (2008) DNA damage-induced upregulation of miR-709 in the germline downregulates BORIS to counteract aberrant DNA hypomethylation. *Cell Cycle*, **7**, 3731-6.
26. Ilnytskyy, Y., Zemp, F.J., Koturbash, I. and Kovalchuk, O. (2008) Altered microRNA expression patterns in irradiated hematopoietic tissues suggest a sex-specific protective mechanism. *Biochem Biophys Res Commun*, **377**, 41-5.
27. Koturbash, I., Boyko, A., Rodriguez-Juarez, R., McDonald, R.J., Tryndyak, V.P., Kovalchuk, I., Pogribny, I.P. and Kovalchuk, O. (2007) Role of epigenetic effectors in maintenance of the long-term persistent bystander effect in spleen in vivo. *Carcinogenesis*, **28**, 1831-8.
28. Boelsma, E., Gibbs, S., Faller, C. and Ponec, M. (2000) Characterization and comparison of reconstructed skin models: morphological and immunohistochemical evaluation. *Acta Derm Venereol*, **80**, 82-8.
29. Ziegler, A., Rockel, B., Hegerl, R., Freitag, B., Lucken, U. and Plitzko, J.M. (2009) Aberration-corrected microscopy for structural biology applications. *J Microsc*, **233**, 170-7.
30. Bonner, W.M., Redon, C.E., Dickey, J.S., Nakamura, A.J., Sedelnikova, O.A., Solier, S. and Pommier, Y. (2008) GammaH2AX and cancer. *Nat Rev Cancer*, **8**, 957-67.
31. Kovalchuk, O., Filkowski, J., Meservy, J., Ilnytskyy, Y., Tryndyak, V.P., Chekhun, V.F. and Pogribny, I.P. (2008) Involvement of microRNA-451 in resistance of the MCF-7 breast cancer cells to chemotherapeutic drug doxorubicin. *Mol Cancer Ther*, **7**, 2152-9.
32. Bolstad, B.M., Irizarry, R.A., Astrand, M. and Speed, T.P. (2003) A comparison of normalization methods for high density oligonucleotide array data based on variance and bias. *Bioinformatics*, **19**, 185-93.
33. Eisen, M.B., Spellman, P.T., Brown, P.O. and Botstein, D. (1998) Cluster analysis and display of genome-wide expression patterns. *Proc Natl Acad Sci U S A*, **95**, 14863-8.
34. Rogakou, E.P., Pilch, D.R., Orr, A.H., Ivanova, V.S. and Bonner, W.M. (1998) DNA double-stranded breaks induce histone H2AX phosphorylation on serine 139. *J Biol Chem*, **273**, 5858-68.
35. O'Donnell, K.A., Wentzel, E.A., Zeller, K.I., Dang, C.V. and Mendell, J.T. (2005) c-Myc-regulated microRNAs modulate E2F1 expression. *Nature*, **435**, 839-43.
36. Petrocca, F., Vecchione, A. and Croce, C.M. (2008) Emerging role of miR-106b-25/miR-17-92 clusters in the control of transforming growth factor beta signaling. *Cancer Res*, **68**, 8191-4.

37. Mendell, J.T. (2008) miRiad roles for the miR-17-92 cluster in development and disease. *Cell*, **133**, 217-22.
38. Matsumura, I., Tanaka, H. and Kanakura, Y. (2003) E2F1 and c-Myc in cell growth and death. *Cell Cycle*, **2**, 333-8.
39. Volinia, S., Calin, G.A., Liu, C.G., Ambs, S., Cimmino, A., Petrocca, F., Visone, R., Iorio, M., Roldo, C., Ferracin, M., Prueitt, R.L., Yanaihara, N., Lanza, G., Scarpa, A., Vecchione, A., Negrini, M., Harris, C.C. and Croce, C.M. (2006) A microRNA expression signature of human solid tumors defines cancer gene targets. *Proc Natl Acad Sci U S A*, **103**, 2257-61.
40. Leiderman, Y.I., Kiss, S. and Mukai, S. (2007) Molecular genetics of RB1--the retinoblastoma gene. *Semin Ophthalmol*, **22**, 247-54.
41. Calin, G.A., Dumitru, C.D., Shimizu, M., Bichi, R., Zupo, S., Noch, E., Aldler, H., Rattan, S., Keating, M., Rai, K., Rassenti, L., Kipps, T., Negrini, M., Bullrich, F. and Croce, C.M. (2002) Frequent deletions and down-regulation of micro- RNA genes miR15 and miR16 at 13q14 in chronic lymphocytic leukemia. *Proc Natl Acad Sci U S A*, **99**, 15524-9.
42. Mott, J.L., Kobayashi, S., Bronk, S.F. and Gores, G.J. (2007) mir-29 regulates Mcl-1 protein expression and apoptosis. *Oncogene*, **26**, 6133-40.
43. Knoepfler, P.S. (2007) Myc goes global: new tricks for an old oncogene. *Cancer Res*, **67**, 5061-3.
44. Coller, H.A., Forman, J.J. and Legesse-Miller, A. (2007) "Myc'ed messages": myc induces transcription of E2F1 while inhibiting its translation via a microRNA polycistron. *PLoS Genet*, **3**, e146.
45. Nieminen, A.I., Partanen, J.I., Hau, A. and Klefstrom, J. (2007) c-Myc primed mitochondria determine cellular sensitivity to TRAIL-induced apoptosis. *Embo J*, **26**, 1055-67.
46. Nieminen, A.I., Partanen, J.I. and Klefstrom, J. (2007) c-Myc blazing a trail of death: coupling of the mitochondrial and death receptor apoptosis pathways by c-Myc. *Cell Cycle*, **6**, 2464-72.
47. Bissonnette, R.P., Echeverri, F., Mahboubi, A. and Green, D.R. (1992) Apoptotic cell death induced by c-myc is inhibited by bcl-2. *Nature*, **359**, 552-4.
48. Chen, T., Wang, Q., Cui, J., Yang, W., Shi, Q., Hua, Z., Ji, J. and Shen, P. (2005) Induction of apoptosis in mouse liver by microcystin-LR: a combined transcriptomic, proteomic, and simulation strategy. *Mol Cell Proteomics*, **4**, 958-74.
49. Huang, X., Lin, T., Gu, J., Zhang, L., Roth, J.A., Liu, J. and Fang, B. (2003) Cell to cell contact required for bystander effect of the TNF-related apoptosis-inducing ligand (TRAIL) gene. *Int J Oncol*, **22**, 1241-5.
50. Shareef, M.M., Cui, N., Burikhanov, R., Gupta, S., Satishkumar, S., Shajahan, S., Mohiuddin, M., Rangnekar, V.M. and Ahmed, M.M. (2007) Role of tumor necrosis factor-alpha and TRAIL in high-dose radiation-induced bystander signaling in lung adenocarcinoma. *Cancer Res*, **67**, 11811-20.
51. Azzam, E.I., de Toledo, S.M. and Little, J.B. (2001) Direct evidence for the participation of gap junction-mediated intercellular communication in the transmission of damage signals from alpha -particle irradiated to nonirradiated cells. *Proc Natl Acad Sci U S A*, **98**, 473-8.
52. van Rooij, E., Marshall, W.S. and Olson, E.N. (2008) Toward microRNA-based therapeutics for heart disease: the sense in antisense. *Circ Res*, **103**, 919-28.
53. Elmen, J., Lindow, M., Schutz, S., Lawrence, M., Petri, A., Obad, S., Lindholm, M., Hedtjarn, M., Hansen, H.F., Berger, U., Gullans, S., Kearney, P., Sarnow, P., Straarup, E.M. and Kauppinen, S. (2008) LNA-mediated microRNA silencing in non-human primates. *Nature*, **452**, 896-9.
54. Sedelnikova, O.A., Redon, C.E., Dickey, J.S., Nakamura, A.J., Georgakilas, A.G. and Bonner, W.M. Role of oxidatively induced DNA lesions in human pathogenesis. *Mutat Res*.

55. Simone, N.L., Soule, B.P., Ly, D., Saleh, A.D., Savage, J.E., Degraff, W., Cook, J., Harris, C.C., Gius, D. and Mitchell, J.B. (2009) Ionizing radiation-induced oxidative stress alters miRNA expression. *PLoS One*, **4**, e6377.
56. Guo, C.J., Pan, Q., Li, D.G., Sun, H. and Liu, B.W. (2009) miR-15b and miR-16 are implicated in activation of the rat hepatic stellate cell: An essential role for apoptosis. *J Hepatol*, **50**, 766-78.
57. Xia, H., Qi, Y., Ng, S.S., Chen, X., Chen, S., Fang, M., Li, D., Zhao, Y., Ge, R., Li, G., Chen, Y., He, M.L., Kung, H.F., Lai, L. and Lin, M.C. (2009) MicroRNA-15b regulates cell cycle progression by targeting cyclins in glioma cells. *Biochem Biophys Res Commun*, **380**, 205-10.
58. Xia, L., Zhang, D., Du, R., Pan, Y., Zhao, L., Sun, S., Hong, L., Liu, J. and Fan, D. (2008) miR-15b and miR-16 modulate multidrug resistance by targeting BCL2 in human gastric cancer cells. *Int J Cancer*, **123**, 372-9.

FIGURE LEGENDS:

Figure 1: Tissue dimensions and irradiation set-up. A narrow α-particle beam irradiated the EpiAirway tissue through the membrane to deliver ~5 α-particles to the nucleus of each cell in a single plane across the tissue base. Bystander tissues were harvested on either side of the irradiated plane for the microarray experiments.

Figure 2: Heat map of ANOVA ($p<0.05$) expression analysis for all treatments. Vertical columns denote days after irradiation for the mock treatment and the bystander tissues (BS). CT–unirradiated sample. The white box includes co-regulated members of the miR-17-92 family. Red boxes highlight important miRNAs discussed in the article. Each line represents an independent biological replicate.

Figure 3: Upregulation of cMYC levels in bystander tissues. Samples were loaded in a random manner to insure lack of bias. For presentation purposes, after scanning pictures were arranged in the following order: mock 8 h; bystander 8h; mock 3d; bystander 3d; bystander 5d. BS – bystander; 8h – 8 hours after irradiation; 3d – 3 days after irradiation; 5d - 5 days after irradiation.

Figure 4: Altered expression of miRNA targets in bystander cells. Samples were loaded in a random manner to insure lack of bias. For presentation purposes, after scanning pictures were arranged in the following order: mock 8 h; bystander 8h; mock 3d; bystander 3d; bystander 5d. BS – bystander; 8h – 8 hours after irradiation; 3d – 3 days after irradiation; 5d - 5 days after irradiation.

Figure 5: Increase of apoptotic cells in bystander tissues following microbeam irradiation. IR-induced apoptotic cell death was scored in side areas of the sections containing unirradiated bystander cells; *Significantly different from the control, $p<0.05$, Student's *t*-test. Cells positive for cleaved caspase-3 were recorded at various times post-IR in Air-100 epithelium. Representative images of apoptotic cells in Air-100 bystander epithelium positive for both cleaved caspase-3 (red) and γ-H2AX (green),10 μm frozen sections, 40x, oil immersion. Cleaved caspase-3 is stained with Alexa 546 (red), γ-H2AX is stained with Alexa 488 (green).

Figure 6: MiRNAs that are involved in regulation of important bystander effect endpoints by targeting crucial regulator proteins.

Supplementary Figure 1: The incidence of γ-H2AX foci in microbeam-irradiated (center) and bystander (side) regions of Air-100 tissue models. Average numbers of γ-H2AX foci per cell and standard errors are shown in the lower left corners. Representative images show the presence of irradiation-induced and bystander foci at different time points post-IR in corresponding tissues. Central layers of the tissues are the mix of irradiated and bystander cells and therefore exhibit the biphasic focal dynamics with two distinguished maxima, 1-2 hrs and 2-5 days post-IR. In contrast, γ-H2AX foci in the distant from the irradiated layer side bystander regions of the tissues only peak at 2-5 days post-IR. The focal numbers decrease by 7 days post-IR in the bystander cells from both central and side regions. Green, γ-H2AX; red, PI; yellow, non-specific membrane staining with both dyes. Magnification, 400x.

Supplementary Figure 2: Altered expression of the miR-17-92 family in bystander tissues.

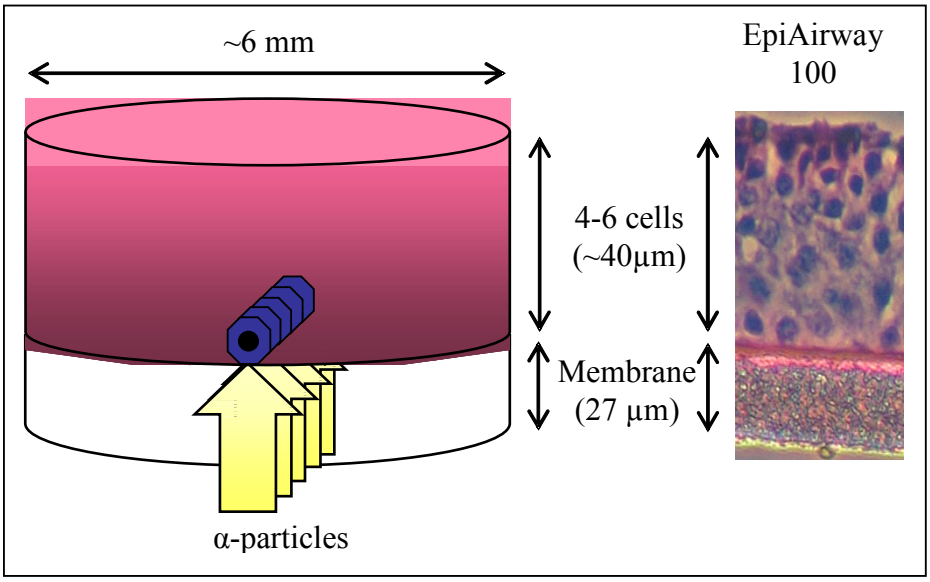

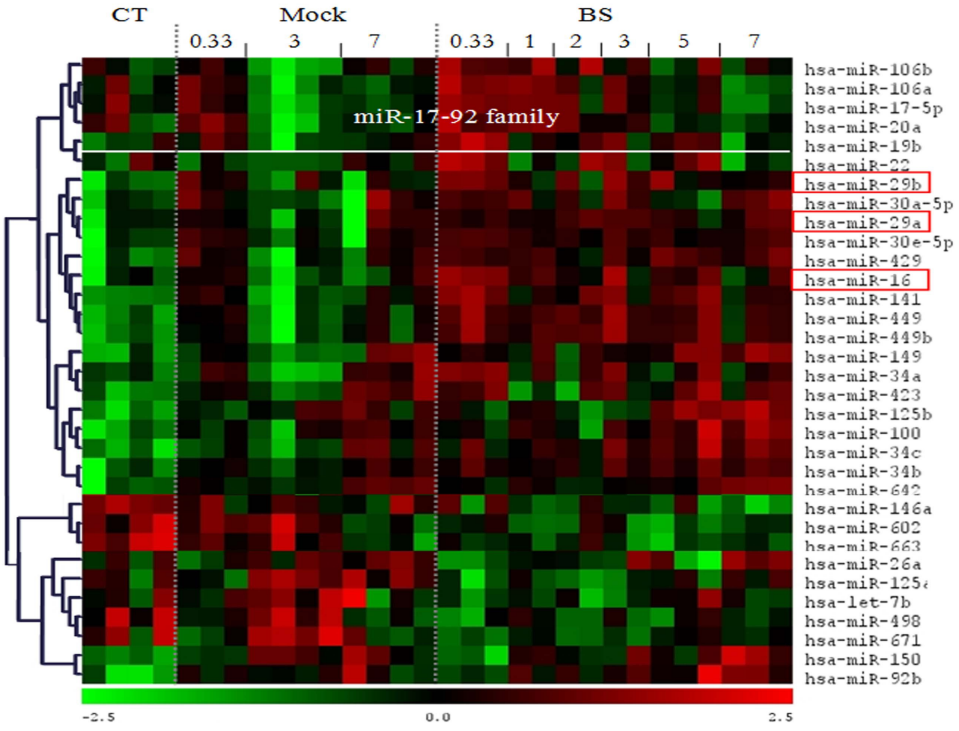

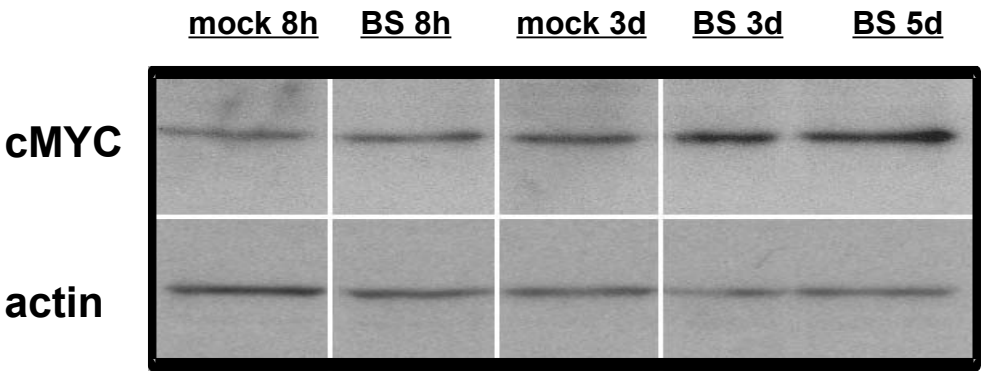

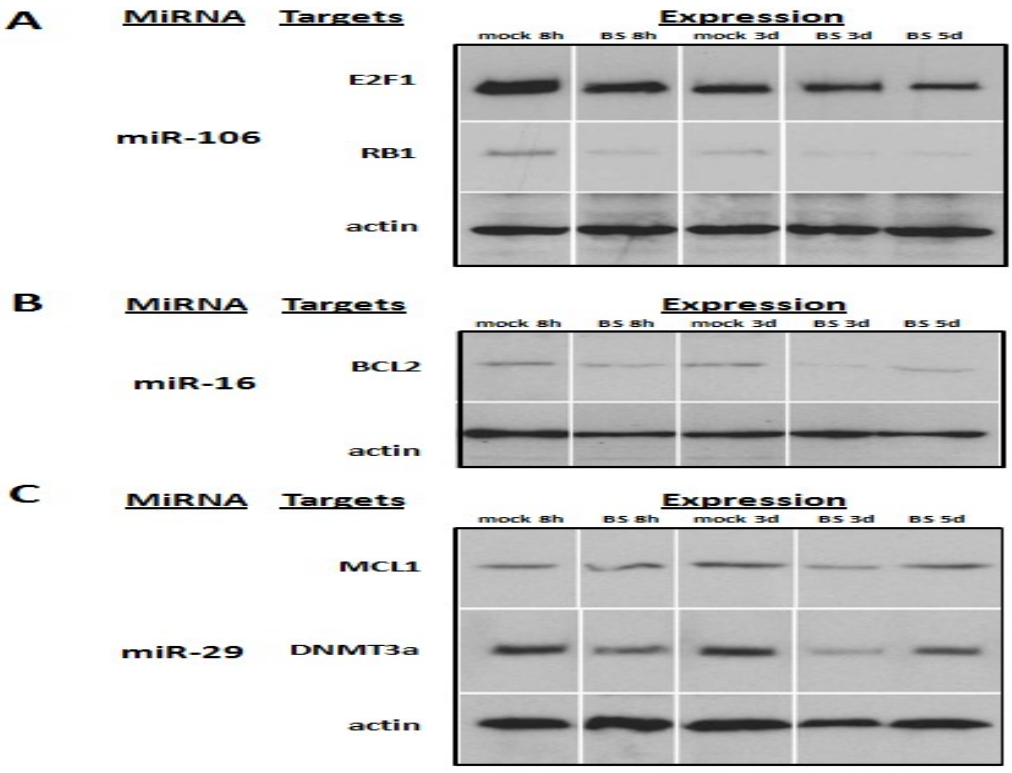

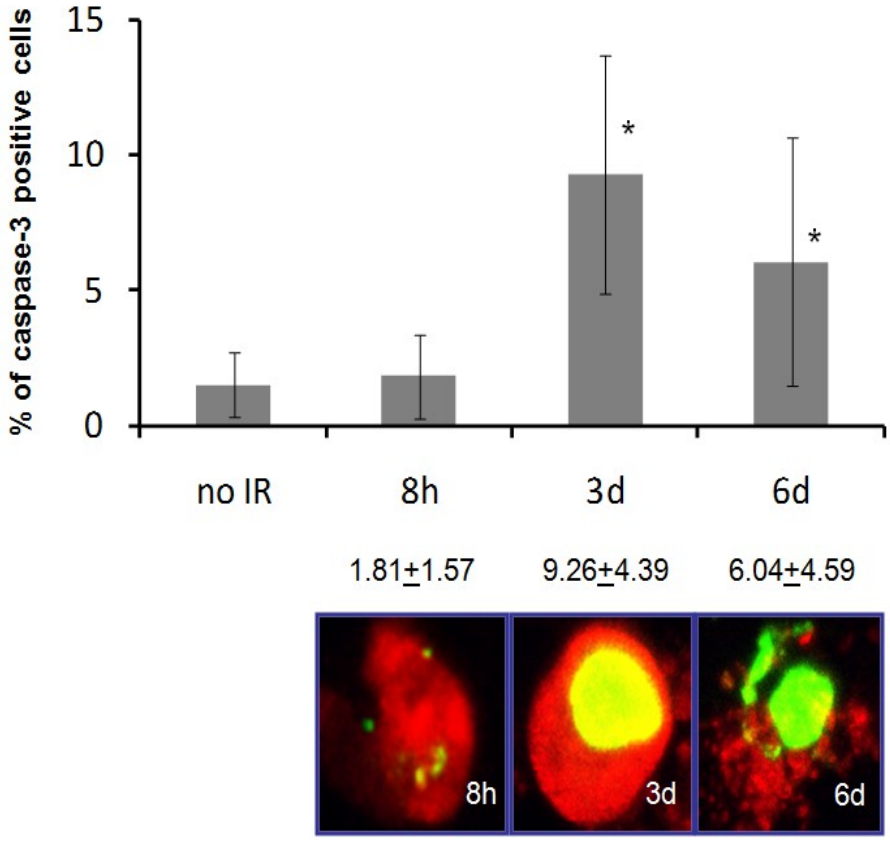

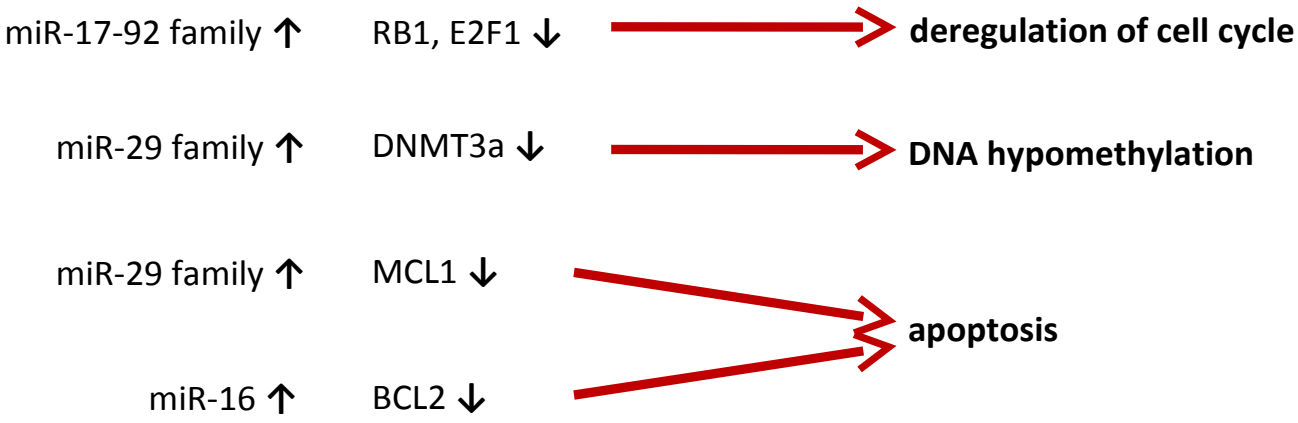

Table 1: Significantly regulated miRNAs in bystander tissue when compared to time-matched controls.

Days Post Irradiation	miRNA	Fold Induction
8 hours	hsa-miR-22	1.95
	hsa-miR-141	1.79
	hsa-miR-16	1.20
	hsa-miR-183	-1.31
3 days	hsa-miR-29c	2.45
	hsa-miR-29a	1.62
	hsa-miR-30a-5p	1.47
	hsa-miR-20a	1.25
	hsa-miR-146a	-1.26
	hsa-miR-125b	-1.18
7 days	hsa-miR-181a	-1.50
	hsa-miR-181b	-1.14

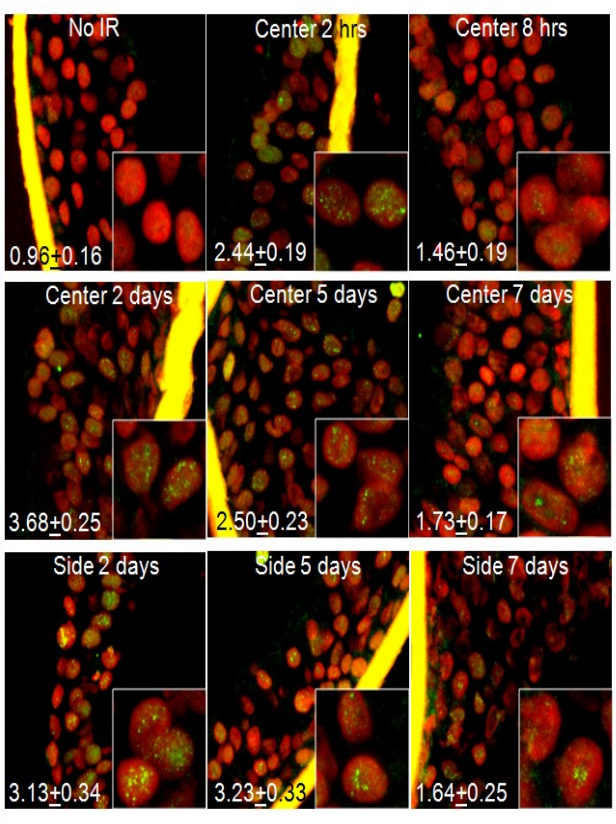

Supplementary Fig. 1.

The incidence of γ-H2AX foci in microbeam-irradiated (center) and bystander (side) regions of Air-100 tissue models. Average numbers of γ-H2AX foci per cell and standard errors are shown in the lower left corners. Representative images show the presence of irradiation-induced and bystander foci at different time points post-IR in corresponding tissues. Central layers of the tissues are the mix of irradiated and bystander cells and therefore exhibit the biphasic focal dynamics with two distinguished maxima, 1-2 hrs and 2-5 days post-IR. In contrast, γ-H2AX foci in the distant from the irradiated layer side bystander regions of the tissues only peak at 2-5 days post-IR. The focal numbers decrease by 7 days post-IR in the bystander cells from both central and side regions. Green, γ-H2AX; red, PI; yellow, non-specific membrane staining with both dyes. Magnification, 400x.